Anthropogenic Hg Emissions, Mg/yr

1000

100

10

1990 1995 2000 2005 2010 2015

> 3000 km

< 3000 km

Hg Concentration, ng/m³

2.0
1.8
1.6
1.4
1.2
1.0

1990 1995 2000 2005 2010 2015

Vermont 99

New York 20

Hg concentrations linked to regional emissions declines

Table of Contents
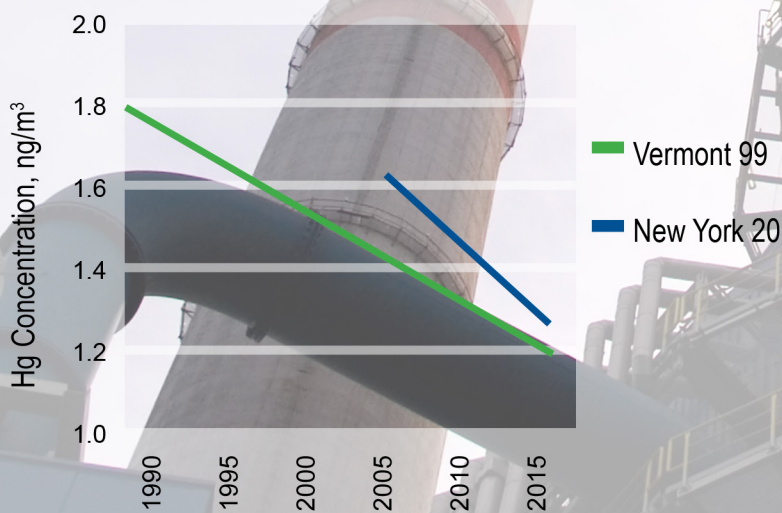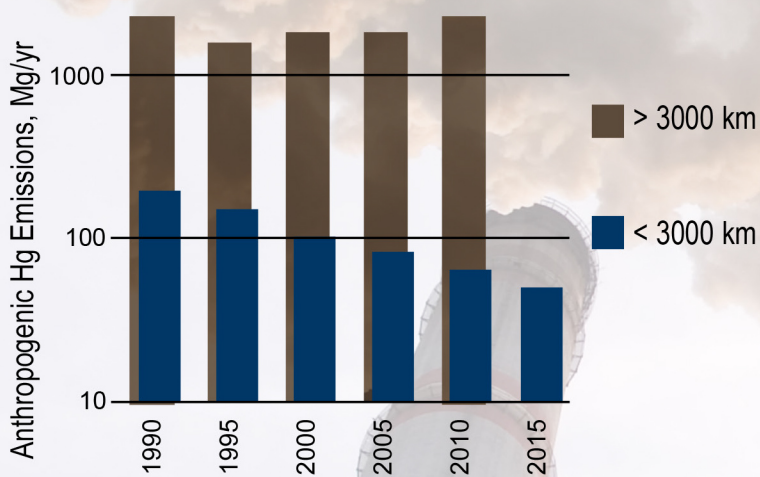

ENVIRONMENTAL Science & Technology LETTERS

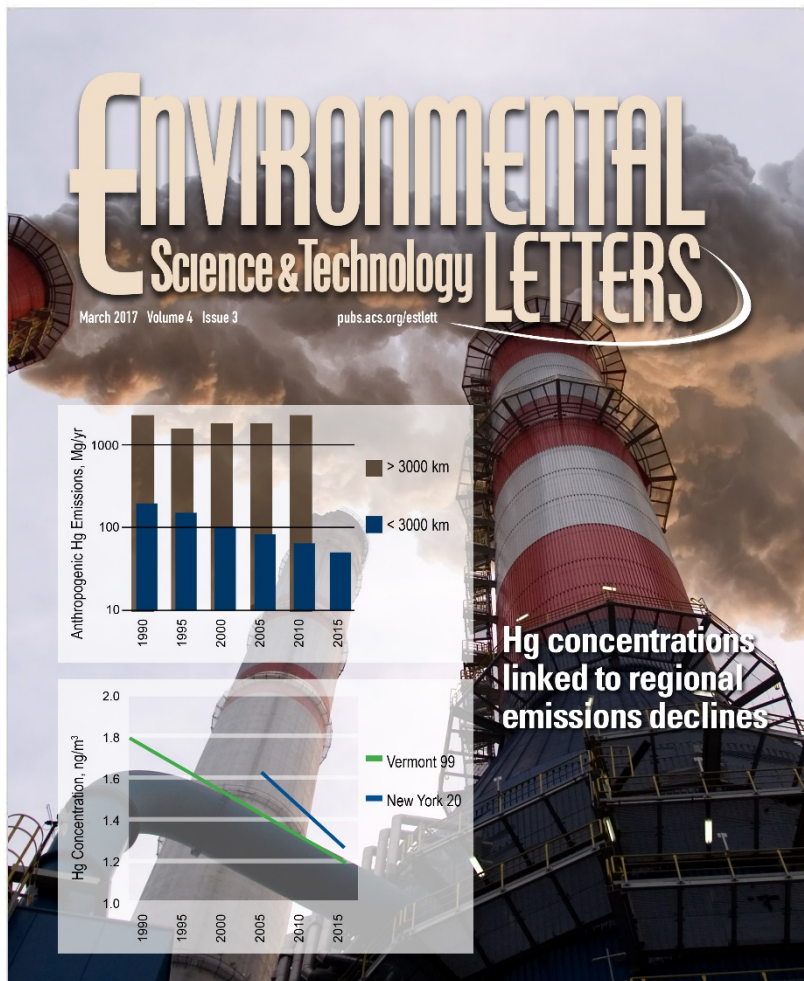March 2017   Volume 4   Issue 3   pubs.acs.org/estlett

Hg concentrations linked to regional emissions declines

ACS Publications
Most Trusted. Most Cited. Most Read.

www.acs.org

About the Cover:
Trends in long-term atmospheric mercury measurements at Underhill, VT, and Huntington Forest, NY, which are generally downwind of large Hg sources in the midwestern United States, indicate that decreased mercury concentrations measured during the past decade are consistent with decreased emissions of Hg from regional point sources and that increasing global emissions have not overwhelmed those decreases.

View the article.

Atmospheric Mercury Temporal Trends in the Northeastern United States from 1992 to 2014: Are Measured Concentrations Responding to Decreasing Regional Emissions?

Hao Zhou,[†] Chuanlong Zhou,[‡] Mary M. Lynam,[§] J. Timothy Dvonch,[§] James A. Barres,[§] Philip K. Hopke,[†] Mark Cohen,[‖] and Thomas M. Holsen*,[‡]

[†]Institute for a Sustainable Environment, Clarkson University, Potsdam, New York 13676, United States
[‡]Department of Civil and Environmental Engineering, Clarkson University, Potsdam, New York 13676, United States
[§]University of Michigan Air Quality Laboratory, Ann Arbor, Michigan 48109, United States
[‖]Air Resources Laboratory, U.S. National Oceanic and Atmospheric Administration, College Park, Maryland 20740, United States

S *Supporting Information*
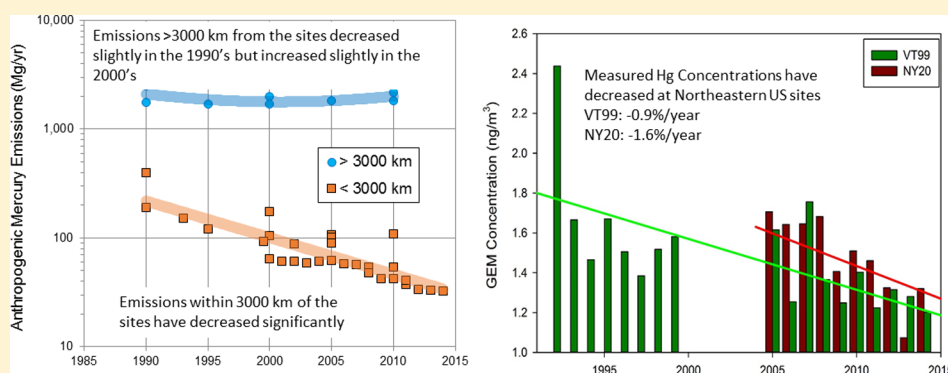
ABSTRACT: Long-term atmospheric mercury measurements at Underhill, VT (VT99), and Huntington Forest, NY (NY20), from 1992 to 2014 and 2005 to 2014, respectively, were used to determine concentration trends using Mann–Kendall's tau test with Sen's slope estimator. These data, measured generally downwind of large Hg sources in the Midwestern United States, provide the longest record of ambient Hg concentrations available in the United States. At VT99, concentrations of gaseous element mercury (GEM), gaseous oxidized mercury (GOM), and particle-bound mercury (PBM) declined at rates of −1.8, −3.2, and −6.7%/year, respectively. At NY20, GEM and GOM concentrations declined at rates of −1.6 and −7.8%/year, respectively; however, PBM concentrations increased at a rate of 2.0%/year, which is likely related to winter wood burning. A trajectory ensemble analysis using the potential source contribution function indicates the source locations associated with high mercury concentrations changed from Toronto–Buffalo and Pennsylvania areas to east coast urban centers. The declining GEM concentrations in the northeastern United States are positively correlated with decreasing SO_2 emissions in the upwind area. Overall, the results indicate that decreased mercury concentrations measured during the past decade are consistent with decreased Hg emissions from regional point sources and that increasing global emissions have not overwhelmed those decreases.

■ INTRODUCTION

Anthropogenic mercury emissions can be direct (e.g., from an active process) or indirect such as re-emission after deposition. Direct anthropogenic mercury emissions in the United States have declined from the early to mid 1990s to the present, due to efforts to reduce mercury in waste streams, added pollution control equipment, and the closure of many waste incinerators and coal burning facilities.[1−4] Further reductions in North American mercury emissions are expected because of recent regulations[5] and economic drivers. However, emissions from countries in Asia such as China and India have increased in part because of rapidly increasing energy consumption.[3,6−8]

There have been previous analyses of atmospheric mercury concentration trends for the United States[2,9] but not for

periods that are as extensive as those presented here. For example, Castro et al.[1] found annual average atmospheric concentrations of gaseous elemental mercury (GEM), gaseous oxidized mercury (GOM), and particle-bound mercury (PBM) in western Maryland declined between 2006 and 2015 and were strongly correlated with power plant Hg emissions from upwind states. Weiss-Penzias et al.[10] merged GEM concentrations from the NADP Atmospheric Hg Network (AMNet) and Environment Canada (EC) networks (CAMNet and

Table 1. Trend Summary for Two Sites from 1992 to 2014

		GEM		GOM		PBM	
site	year	Sen's slope (%/year)[a]	Kendall's tau coefficient[b]	Sen's slope (%/year)[a]	Kendall's tau coefficient[b]	Sen's slope (%/year)[a]	Kendall's tau coefficient[b]
VT99	1992−2014	−0.89(−1.15,−0.74)	−0.291, $p < 0.01$			−1.78(−2.19,−0.83)	−0.23, $p = 0.071$
	1992−1999	−3.22(−4.91,−1.81)	−0.277, $p < 0.01$			−2.81(−7.4,3.43)	−0.060, $p < 0.01$
	2005−2014	−1.76(−2.59,−0.39)	−0.027, $p < 0.01$	−3.19(−4.36,6.96)	−0.281, $p < 0.01$	−6.67(−7.65,−5.26)	−0.026, $p < 0.01$
	2005−2008	−0.51(−1.23,−0.17)	−0.053, $p < 0.01$	−6.88(−7.48,−6.09)	−0.017, $p = 0.397$	−2.12(−6.13,4.02)	−0.024, $p = 0.225$
	2009−2014	−4.16(−6.05,−2.38)	−0.318, $p < 0.01$	−11.50(−14.47,−4.35)	−0.159, $p < 0.01$	−4.22(−10.18,6.22)	−0.072, $p < 0.01$
NY20	2005−2014	−1.56(−2.70,−1.03)	−0.151, $p < 0.01$	−7.79(−9.94,−5.37)	−0.197, $p < 0.01$	1.97(−3.91,15.4)	0.009, $p = 0.051$
	2005−2008	−3.37(−7.41,3.89)	−0.148, $p < 0.01$	−18.46(−23.95,−9.52)	−0.320, $p < 0.01$	−10.13(−13.96,−1.44)	−0.309, $p < 0.01$
	2009−2014	−1.00(−2.74,1.17)	−0.052, $p < 0.05$	−7.06(−11.21,2.16)	−0.095, $p < 0.01$	4.08(1.55,5.36)	0.138, $p < 0.01$

[a]Two numbers in parentheses indicate upper 95% and lower 95% slopes. [b]Kendall's tau coefficient (from −1 to 1) indicating the slope of the trend. $p < 0.05$ indicates the trend is statistically significant, and $p < 0.01$ indicates the trend is very significant.

NatChem) and found that there was a significant negative trend during 1998−2007, but no significant trend was observed for the period 2008−2013 across the United States and Canada.

In an effort to improve our understanding of atmospheric speciated mercury trends and their relationship to regional and global sources, an analysis of speciated atmospheric mercury monitoring data at three sites in the northeastern United States was conducted. Data from these sites represent the longest ambient Hg data record available in the United States. These types of long data records are important for understanding Hg cycling in the environment because the long residence time of some Hg species results in slow changes in ambient concentrations. In addition, regional emissions, which influence Hg signals, have been declining for several decades. The sites are generally downwind of large U.S. source regions and are in ideal locations for investigation of the influence of regional and global emissions on Hg concentrations in the central and northeastern United States.

■ MATERIALS AND METHODS

Sites and Data Sources. Data from the Underhill, VT (VT99) (44.51N, −72.91W), Huntington Forest, NY (NY20) (43.97N, −74.22W), and Potsdam, NY (44.67N, −74.98W), sites were used in this analysis (Figure S1). A combination of manual and automated Tekran measurement techniques were used following strict QA/QC protocols (see the Supporting Information for details).

Trend Analysis. Raw atmospheric mercury concentration data were converted into daily median values to calculate pairwise slopes. These raw data were adjusted by a seasonal trend decomposition procedure based on loess (STL)[11] to reduce seasonal effects. Bootstrap resampling was applied to increase parameter estimate robustness[12] and provide an estimate of the p value for the slope. Kendall's tau coefficients were also calculated for each time period. Additional information can be found in the Supporting Information. Seasonal trends are shown in Figure S2.

Stepwise multiple regression[13,14] and non-negative least-squares analysis[15] were applied to 2004−2014 GEM concentration data from the NY20 and VT99 sites and sulfur dioxide emission data from upwind states and Ontario Canada collected by the U.S. Environmental Protection Agency as Air Market Program Data. Only variables with non-negative coefficients were included because negative terms are not physically realistic.

Source Analysis. JP-PSCF (Joint Point Potential Source Contribution Function) is often used for multisite measurements using trajectories pooled using the following:

$$\text{PSCF}(\text{JP}_{ij}) = \frac{\text{PSCF}_{\text{site A}}(m_{ij}) + \text{PSCF}_{\text{site B}}(m_{ij})}{\text{PSCF}_{\text{site A}}(n_{ij}) + \text{PSCF}_{\text{site B}}(n_{ij})} \quad (1)$$

Three-day backward trajectories were calculated at the midpoint of every 3 h sample for continuous Tekran data obtained during the period from 2004 to 2014 and every 6 h for 24 h samples collected during the period from 1992 to 1999 using the NOAA HYSPLIT-4 model.[16,17] Additional information can be found in the Supporting Information.

■ RESULTS AND DISCUSSION

GEM Trends. Over the 22 years of measurements, the overall Sen's slope for GEM concentration for VT99 is −0.89%/year (Table 1 and Figure 1) (p values for all reported trends were at a level of <0.01 unless otherwise indicated; confidence intervals are listed in Table 1). The GEM concentration trends from the period of January 2005 to December 2014 at VT99 and NY20 (Table 1 and Figure 1) were both negative with somewhat larger rates of −1.8 and −1.6%/year, respectively. The annual average GEM concentration, measured intermittently at Potsdam, dropped from 2.0 ± 1.3 to 1.4 ± 0.2 ng/m³ for the years 2004−2005 and 2013−2014. Divided into three separate time periods, the VT99 GEM trend was significantly negative from 1992 to 1999 and from 2009 to 2014 (−3.2 and −4.2%/year, respectively). However, the GEM trend was relatively constant from 2005 to 2008 with a declining rate of −0.51%/year. For NY20, the GEM concentration decreased fastest from 2005 to 2008 with a rate of −3.4%/year and slowly decreased from 2009 to 2014 with a rate of −1.0%/year ($p < 0.05$).

Analysis of Hg emission inventories (Figures S3−S5 and S7−S9) show that "regional-scale" (<600 km) and "continental-scale" (600−3000 km) direct anthropogenic mercury emissions
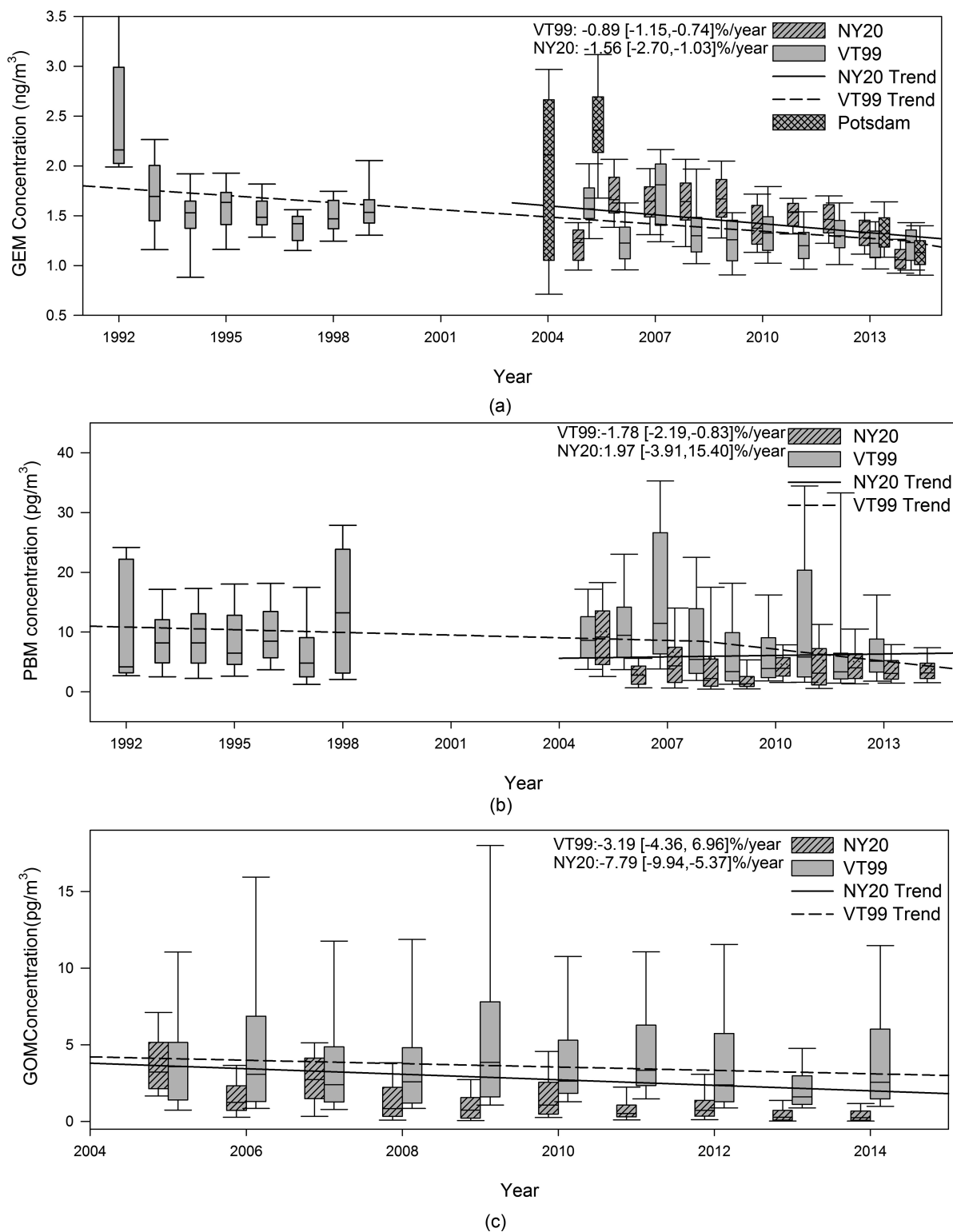
Figure 1. (a) GEM trends from 1992 to 2014 for the Underhill, VT (VT99), Huntington, NY (NY20), and Potsdam, NY, sites and (b) PBM trends and (c) GOM trends from 2005 to 2014 for the VT99 and NY20 sites.

decreased significantly from 1990 to 2014, in part because of mercury control policies.[18] Emission reductions during the 1990s, driven largely by decreasing waste incineration emissions, were generally greater than those in the 2000s, driven largely by reductions in coal-fired power plant emissions. In contrast, "global-scale" mercury emissions (>3000 km from the sites) generally decreased from 1990 to 2000 but then

increased from 2000 to 2010 (Figure S6). The negative trends in GEM concentrations since 1992 are consistent with trends in regional and continental emissions. The GEM decrease was more pronounced during the 1990s than during the 2000s, consistent with the larger reduction in regional emissions particularly within 600 km of the sites during the 1990s. However, impacts from changing global emissions on these

decadal decreasing trends cannot be discounted. The decreasing global emissions during the 1990s could have reinforced the concurrent regional/continental emissions decreases leading to a steeper concentration decline, while the increasing global emissions during the 2000s could have partially counterbalanced the concurrent regional/continental emissions decreases, leading to a more modest decreasing concentration trend.

NY20 GEM concentrations declined faster during 2004–2008 than during 2009–2014, in contrast to the change in trend magnitudes for the two periods at VT99. The decline in emissions within 600 km of NY20 was steeper over 2004–2008 than that for VT99 (Figure S5c), and this steeper decline may partly explain this difference.

GOM Trends. GOM concentrations (2005–2014) showed significant negative trends with rates of −3.2 and −7.8%/year (Figure 1) for VT99 and NY20, respectively. At VT99, the slope was more negative for the period of 2009–2014 than for the period of 2005–2008, but the relative rates of the two periods were reversed for NY20. Recent research has indicated that ozone and water vapor can cause artifacts in GOM measurements.[19,20] The possible influence of these artifacts on trend analysis was discussed in detail by Ren et al.,[21] who found that these artifacts at their site were unlikely to impact trend analysis because biases were likely to be consistent. To further explore this possibility, ozone concentrations (data from the CASTNET network for Huntington, NY, and EPA AirData AQI data for Underhill, VT) were examined and found to have decreased at a rate much smaller than that of GOM (−0.7 and −1.1%/year vs −6.9 and −7.8%/year for VT99 and NY20, respectively).[21]

Speciated emissions trends over this period are not well-known because global, speciated inventories are available through only 2010;[22,23] more frequently updated U.S. and Canadian national inventories are generally not speciated. However, decreasing emissions over the period of 2005–2014 in the Ohio River Valley (ORV) (Figures S8–9) arose in part due to installation of SO_2 controls on coal-fired plants that concomitantly reduced GOM emissions as a co-benefit and in part due to reduced coal combustion (e.g., in favor of natural gas combustion). As a result of both of these factors, GOM emissions were likely reduced significantly over this period. NY20 is ∼120 km closer to the ORV region than VT99 is, corresponding to a ∼0.5 day difference in atmospheric transport time. Because the atmospheric lifetime of GOM in the planetary boundary layer is on the order of days due to dry and wet deposition, a difference of ∼0.5 day may be significant. Moreover, plume dilution will increase with distance from the source. Thus, NY20 may have been more sensitive to the emissions decreases in the ORV region, contributing to its greater decrease in GOM concentrations.

Weiss-Penzias et al.[10] found that between 2001 and 2013, four of the eight sites in the upper ORV and Pennsylvania showed significant negative trends in mercury concentration in precipitation, one had a significant positive trend, and three had no trend, largely consistent with the decrease in GOM sources in the region. Thiel-Sen trend analysis using the entire MDN data record at NY20 and VT99 individually found that the mercury concentration in precipitation decreased at −1.8%/year between 1999 and 2015 at NY20 and at the same rate over the period from 2004 to 2015 at VT99 (Figure S10).

PBM Trends. PBM concentrations at the VT99 site for the periods of 1992–1999 and 2004–2014 yielded an overall trend

of −1.8%/year (Figure 1). Considering time periods separately, trends for 1992–1999, 2005–2008, and 2009–2014 were −2.8, −2.1, and −4.2%/year, respectively (Table 1 and Figure 1). The overall PBM concentration trend at NY20 during the period of 2005–2014 was positive (1.2%/year), whereas at VT99, it was negative (−6.7%/year) (Figure 1). A significant negative trend was found for the VT99 site, and a marginally significant increasing trend was found for the NY20 site ($p =$ 0.051) from 2005 to 2014 (Table 1). Higher monthly PBM concentrations were found in winter at both sites (Figure S2), suggesting local/regional wood burning was a significant source of PBM[24] and reflecting increased condensation of gas phase mercury onto particles during colder seasons.[25] Particle mass concentration trends from 2005 to 2014 were found to be −1.75 and −1.77%/year for VT99 and NY20, respectively.[26] These changes were relatively small, and for some seasons in the opposite direction compared to PBM trends during the same period. These results suggest the trend in PBM concentration is likely mostly due to the variations in atmosphere mercury concentration and not the variation in particle mass concentration.

Atmospheric concentrations of PBM are influenced by primary emissions and atmospheric physical–chemical trans-formations that intraconvert GEM, GOM, and PBM, complicating the interpretation of spatiotemporal trends. Figures S3 and S4 show that primary PBM emissions within 600 and 600–3000 km of the sites decreased by ∼60–80% during the 1990s but only an additional 10% during the 2000s. These decadal trends are consistent with the observed faster concentration decline in the 1990s than in the 2000s. There are conflicting trends in remote PBM emissions (>3000 km) among different inventories (Figure S6), making it difficult to assess their relative importance. PBM concentrations at NY20 decreased over the period of 2005–2008 but increased over the period of 2009–2014, with an overall positive trend over the period of 2005–2014. Figure S5 shows that overall mercury emissions within 600 km and within 3000 km of the sites declined significantly over the period of 2005–2009 but were relatively constant over the period of 2009–2014.

Seasonal Trends (2005–2014). GEM concentration trends at both sites were positive in spring and negative for the other three seasons (Figure S2). [The seasons are defined as winter (December, January, and February), spring (March, April, and May), summer (June, July, and August), and autumn (September, October, and November).] This difference in spring may be due, at least in part, to increasing snowfall and large or more frequent melting of the snowpack that released accumulated Hg.[27−29] GOM concentration trends were positive in the spring and negative in the other three seasons at the VT99 site. However, they decreased during all four seasons at the NY20 site but had smaller negative slopes in the spring and summer. The different trends by season could be ascribed to the more oxidizing environment in the spring and summer under more sunlight and higher temperatures.[30] The less active oxidation processes in the atmosphere in the eastern United States over the past several decades[31,32] may be responsible for the observed changes. The PBM concentration trends in the winter season were 3.0 and 4.2%/year at VT99 and NY20, respectively. The positive trends at the two sites may be related to increases in local wood burning emissions over time because local wood burning in winter is a source of PBM.[24] PBM concentration trends were positive during all seasons at NY20
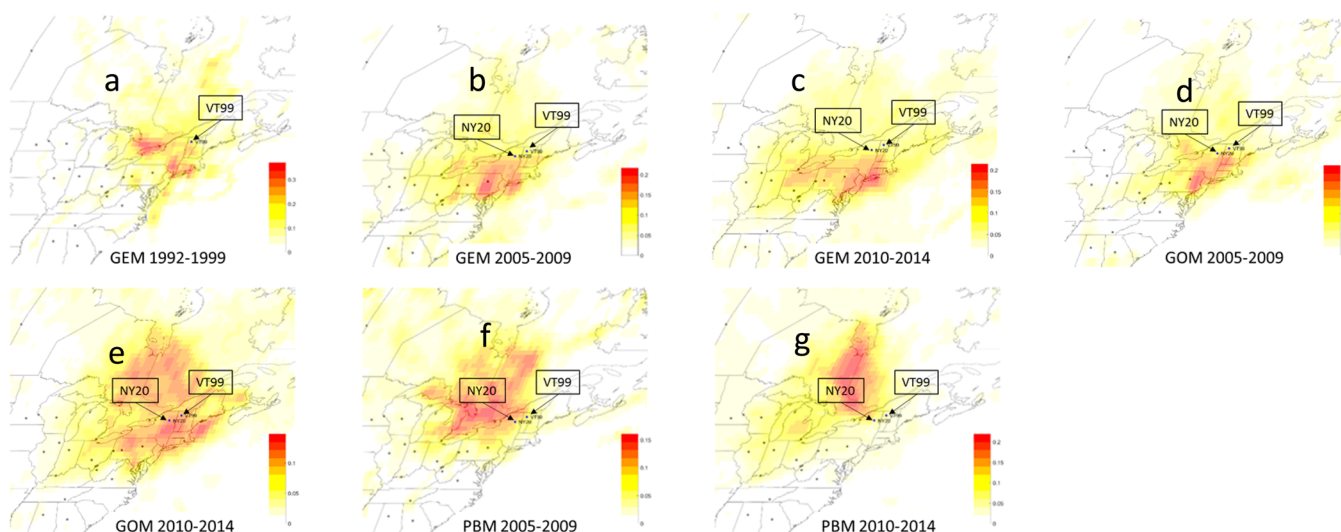
Figure 2. Underhill, VT (VT99), GEM PSCF result for 1992−1999 (a) and Huntington Forest, NY (NY20), and Underhill, VT (VT99), joint-PSCF GEM results for (b) 2005−2009 and (c) 2010−2014, GOM results for (d) 2005−2009 and (e) 2010−2014, and PBM results for (f) 2005−2009 and (g) 2010−2014 with emission sources. The U.S. map was taken from GADM database of Global Administrative Areas.[40]

but positive only during winter and decreasing during other seasons at VT99.

Source Analysis. Joint-PSCF results indicated that the major source areas associated with high GEM concentrations were originally associated with the Toronto−Buffalo region/Pennsylvania and the NYC metro/NJ−Philadelphia−Wilmington area (Figure 2a−c) (1992−1999) and changed to only the east coast region (2010−2014). This change is possibly due to reduced emissions from coal-fired utilities located in Toronto−Buffalo/Pennsylvania regions such as the partial closing of facilities at Nanticoke, ON, in 2008, the shutdown of a 260 MW coal-fired power plant in Rochester, NY, between February and April 2008, and the reduction of waste incineration in and around these large metropolitan areas. For GOM, Pennsylvania and the eastern coastal region were initially the major source locations associated with high concentrations (Figure 2d,e). More recently, locations associated with high GOM concentrations were more evenly distributed as the emissions from the earlier predominant source regions have been sharply reduced. The relative importance of re-emissions of Hg used in commercial products and previously deposited Hg in urban areas[33,34] appears to have increased due to decreases in point source mercury emissions.

PBM PSCF results (Figure 2f,g) showed PBM sources moved to the western Quebec region (Val d'Or area) during the period of 2010−2014 from southern Ontario (Sudbury area) and western Quebec during the period of 2005−2009. This change is consistent with the decreasing emissions in Sudbury due to closure of Falconbridge Ltd. metal refining works in 2006.[35] The change is also consistent with Figures S8 and S9 that show that mercury emissions generally declined over the period of 2005−2014 in regions west of the sites but stayed relatively high north of the sites (e.g., in the Montreal region). Forest fires have also been shown to be a source of PBM in this region, although those are mostly associated with late spring and summer months.[36]

Stepwise multiple-regression analysis between NY20 GEM concentrations and SO_2 emissions showed SO_2 emissions in West Virginia, Pennsylvania, and Ohio were related to GEM concentrations ($r^2 = 0.14$); GEM concentrations at the VT99 site were most associated with SO_2 emissions in West Virginia and Ontario, Canada, during the period of 2004−2014 ($r^2 = 0.25$) (Table S1). The measurement date also was a significant influencing factor at both sites, consistent with the decreasing trends discussed above developed with other statistical methodologies. Non-negative least-square analysis indicated the SO_2 emission areas, which are related to GEM concentrations at the NY20 site, changed from Ohio and West Virginia to Connecticut and West Virginia in the most recent five years. For GEM concentrations at VT99, the influence of SO_2 emissions in West Virginia, New York, Ohio, and Virginia changed to no specific source locations in the most recent five years (Table S2). These changes are consistent with the PSCF results for these two sites and suggest the declines in emissions from power plants are a major cause of negative trends in mercury concentrations in the northeastern area of the United States.[37−39]

■ ASSOCIATED CONTENT

Ⓢ Supporting Information

The Supporting Information is available free of charge on the ACS Publications website at DOI: 10.1021/acs.estlett.6b00452.

Site locations, data sources, trends in different seasons, stepwise multiple-regression and non-negative least-squares regression analysis, mercury emissions analysis, and wet deposition concentration trends (PDF)

■ AUTHOR INFORMATION

Corresponding Author

*E-mail: holsen@clarkson.edu. Phone: 315-268-3851.

ORCID Ⓘ

Thomas M. Holsen: 0000-0001-9599-6733

Notes

The authors declare no competing financial interest.

■ REFERENCES

(1) Castro, M. S.; Sherwell, J. Effectiveness of emission controls to reduce the atmospheric concentrations of mercury. *Environ. Sci. Technol.* **2015**, *49*, 14000–14007.

(2) Butler, T. J.; Cohen, M. D.; Vermeylen, F. M.; Likens, G. E.; Schmeltz, D.; Artz, R. S. Regional precipitation mercury trends in the eastern USA, 1998–2005: Declines in the Northeast and Midwest, no trend in the Southeast. *Atmos. Environ.* **2008**, *42*, 1582–1592.

(3) Pacyna, J. M.; Pacyna, E. G.; Steenhuisen, F.; Wilson, S. Mapping 1995 global anthropogenic emissions of mercury. *Atmos. Environ.* **2003**, *37*, 109–117.

(4) Ambrose, J. L.; Gratz, L. E.; Jaffe, D. A.; Campos, T.; Flocke, F. M.; Knapp, D. J.; Stechman, D. M.; Stell, M.; Weinheimer, A. J.; Cantrell, C. A.; Mauldin, R. L. Mercury emission ratios from coal-fired power plants in the southeastern United States during NOMADSS. *Environ. Sci. Technol.* **2015**, *49*, 10389–10397.

(5) Sunderland, E. M.; Driscoll, C. T., Jr.; Hammitt, J. K.; Grandjean, P.; Evans, J. S.; Blum, J. D.; Chen, C. Y.; Evers, D. C.; Jaffe, D. A.; Mason, R. P.; Goho, S.; Jacobs, W. Benefits of Regulating Hazardous Air Pollutants from Coal and Oil-Fired Utilities in the United States. *Environ. Sci. Technol.* **2016**, *50*, 2117–20.

(6) Burger Chakraborty, L.; Qureshi, A.; Vadenbo, C.; Hellweg, S. Anthropogenic mercury flows in India and impacts of emission controls. *Environ. Sci. Technol.* **2013**, *47*, 8105–8113.

(7) Tian, H.; Zhu, C.; Gao, J.; Cheng, K.; Hao, J.; Wang, K.; Hua, S.; Wang, Y.; Zhou, J. Quantitative assessment of atmospheric emissions of toxic heavy metals from anthropogenic sources in China: historical trend, spatial distribution, uncertainties, and control policies. *Atmos. Chem. Phys.* **2015**, *15*, 10127–10147.

(8) Zhang, L.; Wang, S.; Wang, L.; Wu, Y.; Duan, L.; Wu, Q.; Wang, F.; Yang, M.; Yang, H.; Hao, J.; Liu, X. Updated Emission Inventories for Speciated Atmospheric Mercury from Anthropogenic Sources in China. *Environ. Sci. Technol.* **2015**, *49* (5), 3185–3194.

(9) Risch, M. R.; Gay, D. A.; Fowler, K. K.; Keeler, G. J.; Backus, S. M.; Blanchard, P.; Barres, J. A.; Dvonch, J. T. Spatial patterns and temporal trends in mercury concentrations, precipitation depths, and mercury wet deposition in the North American Great Lakes region, 2002–2008. *Environ. Pollut.* **2012**, *161*, 261–71.

(10) Weiss-Penzias, P. S.; Gay, D. A.; Brigham, M. E.; Parsons, M. T.; Gustin, M. S.; Ter Schure, A. Trends in mercury wet deposition and mercury air concentrations across the U.S. and Canada. *Sci. Total Environ.* **2016**, *568*, 546–556.

(11) Cleveland, R. B.; Cleveland, W. S.; McRae, J. E.; Terpenning, I. STL: A seasonal-trend decomposition procedure based on loess. *Journal of Official Statistics* **1990**, *6*, 3–73.

(12) Berkovits, I.; Hancock, G. R.; Nevitt, J. Bootstrap resampling approaches for repeated measure designs: relative robustness to sphericity and normality violations. *Educ. Psychol. Meas.* **2000**, *60*, 877–892.

(13) Abdul-Wahab, S. A.; Bakheit, C. S.; Al-Alawi, S. M. Principal component and multiple regression analysis in modelling of ground-level ozone and factors affecting its concentrations. *Environ. Mod. & Sof.* **2005**, *20*, 1263–1271.

(14) Monteith, D. T.; Stoddard, J. L.; Evans, C. D.; de Wit, H. A.; Forsius, M.; Høgåsen, T.; Wilander, A.; Skjelkvåle, B. L.; Jeffries, D. S.; Vuorenmaa, J.; Keller, B.; Kopácek, J.; Vesely, J. Dissolved organic carbon trends resulting from changes in atmospheric deposition chemistry. *Nature* **2007**, *450*, 537–540.

(15) Paatero, P. Least squares formulation of robust non-negative factor analysis. *Chemom. Intell. Lab. Syst.* **1997**, *37*, 23–35.

(16) Stein, A.; Draxler, R.; Rolph, G.; Stunder, B.; Cohen, M.; Ngan, F. NOAA's HYSPLIT atmospheric transport and dispersion modeling system. *Bull. Am. Meteorol. Soc.* **2015**, *96*, 2059–2077.

(17) Draxler, R. R.; Hess, G. An overview of the HYSPLIT_4 modelling system for trajectories. *Aust. Meteorol. Mag.* **1998**, *47*, 295–308.

(18) Muntean, M.; Janssens-Maenhout, G.; Song, S.; Selin, N. E.; Olivier, J. G.; Guizzardi, D.; Maas, R.; Dentener, F. Trend analysis from 1970 to 2008 and model evaluation of EDGARv4 global gridded anthropogenic mercury emissions. *Sci. Total Environ.* **2014**, *494–495*, 337–50.

(19) Huang, J.; Miller, M. B.; Weiss-Penzias, P.; Gustin, M. S. Comparison of Gaseous Oxidized Hg measured by KCl-coated Denuders, and Nylon and Cation Exchange Membranes. *Environ. Sci. Technol.* **2013**, *47*, 7307–16.

(20) Lyman, S. N.; Jaffe, D. A.; Gustin, M. S. Release of mercury halides from KCl denuders in the presence of ozone. *Atmos. Chem. Phys.* **2010**, *10*, 8197–8204.

(21) Ren, X.; Luke, W. T.; Kelley, P.; Cohen, M. D.; Artz, R.; Olson, M. L.; Schmeltz, D.; Puchalski, M.; Goldberg, D. L.; Ring, A.; Mazzuca, G. M.; Cummings, K. A.; Wojdan, L.; Preaux, S.; Stehr, J. W. Atmospheric mercury measurements at a suburban site in the Mid-Atlantic United States: Inter-annual, seasonal and diurnal variations and source-receptor relationships. *Atmos. Environ.* **2016**, *146*, 141–152.

(22) Zhang, Y.; Jacob, D. J.; Horowitz, H. M.; Chen, L.; Amos, H. M.; Krabbenhoft, D. P.; Slemr, F.; St. Louis, V. L.; Sunderland, E. M. Observed decrease in atmospheric mercury explained by global decline in anthropogenic emissions. *Proc. Natl. Acad. Sci. U. S. A.* **2016**, *113*, 526–531.

(23) Wilson, S.; Munthe, J.; Sundseth, K.; Maxson, P.; Kindbom, K.; Pacyna, J.; Steenhuisen, F. Updating Historical Global Inventories of Anthropogenic Mercury Emissions to Air. AMAP Technical Report Number 3 (2010); Arctic Monitoring and Assessment Programme (AMAP): Oslo, 2010.

(24) Huang, J.; Hopke, P. K.; Choi, H. D.; Laing, J. R.; Cui, H.; Zananski, T. J.; Chandrasekaran, S. R.; Rattigan, O. V.; Holsen, T. M. Mercury (Hg) emissions from domestic biomass combustion for space heating. *Chemosphere* **2011**, *84*, 1694–9.

(25) Lynam, M. M.; Keeler, G. J. Artifacts associated with the measurement of particulate mercury in an urban environment: The influence of elevated ozone concentrations. *Atmos. Environ.* **2005**, *39*, 3081–3088.

(26) EPA AirData AQI database; U.S. Environmental Protection Agency: Washington, DC, 2016.

(27) Huang, J.; Choi, H.-D.; Hopke, P. K.; Holsen, T. M. Ambient mercury sources in Rochester, NY: results from principle components analysis (PCA) of mercury monitoring network data. *Environ. Sci. Technol.* **2010**, *44*, 8441–8445.

(28) Wetherbee, G. A.; Mast, M. A. Annual variations in wet-deposition chemistry related to changes in climate. *Climate Dynamics* **2016**, *47*, 3141–3155.

(29) Suriano, Z. J.; Leathers, D. J. Twenty-first century snowfall projections within the eastern Great Lakes region: detecting the presence of a lake-induced snowfall signal in GCMs. *Int. J. Climatol.* **2016**, *36* (5), 2200–2209.

(30) Choi, H.-D.; Huang, J.; Mondal, S.; Holsen, T. M. Variation in concentrations of three mercury (Hg) forms at a rural and a suburban site in New York State. *Sci. Total Environ.* **2013**, *448*, 96–106.

(31) Cooper, O. R.; Gao, R. S.; Tarasick, D.; Leblanc, T.; Sweeney, C. Long-term ozone trends at rural ozone monitoring sites across the United States, 1990−2010. *J. Geophys. Res.: Atmos.* **2012**, *117*, n/a.

(32) Strode, S. A.; Rodriguez, J. M.; Logan, J. A.; Cooper, O. R.; Witte, J. C.; Lamsal, L. N.; Damon, M.; Van Aartsen, B.; Steenrod, S. D.; Strahan, S. E. Trends and variability in surface ozone over the United States. *J. Geophys. Res.: Atmos.* **2015**, *120*, 9020−9042.

(33) Gratz, L. In Airborne observations of mercury emissions from the Chicago/Gary urban/industrial area during the 2013 NOMADSS campaign. 2015 AGU Fall Meeting, San Francisco; American Geophysical Union: Washington, DC, 2015.

(34) Horowitz, H. M.; Jacob, D. J.; Amos, H. M.; Streets, D. G.; Sunderland, E. M. Historical mercury releases from commercial products: Global environmental implications. *Environ. Sci. Technol.* **2014**, *48*, 10242−10250.

(35) Hoffman, A. Closed mines broken dreams in the town that nickel built. http://www.theglobeandmail.com/report-on-business/closed-mines-broken-dreams-in-the-town-that-nickel-built/article17975953/ (Accessed Dec. 05, 2008).

(36) Wang, Y.; Huang, J.; Zananski, T. J.; Hopke, P. K.; Holsen, T. M. Impacts of the Canadian forest fires on atmospheric mercury and carbonaceous particles in northern New York. *Environ. Sci. Technol.* **2010**, *44*, 8435−8440.

(37) Pavlish, J. H.; Sondreal, E. A.; Mann, M. D.; Olson, E. S.; Galbreath, K. C.; Laudal, D. L.; Benson, S. A. Status review of mercury control options for coal-fired power plants. *Fuel Process. Technol.* **2003**, *82*, 89−165.

(38) Pacyna, E. G.; Pacyna, J. M.; Steenhuisen, F.; Wilson, S. Global anthropogenic mercury emission inventory for 2000. *Atmos. Environ.* **2006**, *40*, 4048−4063.

(39) Rafaj, P.; Bertok, I.; Cofala, J.; Schoepp, W. Scenarios of global mercury emissions from anthropogenic sources. *Atmos. Environ.* **2013**, *79*, 472−479.

(40) Hijmans, R.; Kapoor, J.; Wieczorek, J.; Garcia, N.; Maunahan, A.; Rala, A.; Mandel, A. *GADM database of Global Administrative Areas*; University of California: Berkeley, CA, 2009.

■ NOTE ADDED AFTER ASAP PUBLICATION

A reference was omitted in the Supporting Information file in the version of this paper published January 6, 2017. The updated file published February 17, 2017.

Supporting Information for

Atmospheric Mercury Temporal Trends in the Northeastern United States from 1992 to 2014: Are Measured Concentrations Responding to Decreasing Regional Emissions?

Hao Zhou[1], Chuanlong Zhou[2], Mary M. Lynam[3], J. Timothy. Dvonch[3], James A. Barres[3], Philip K. Hopke[1], Mark Cohen[4], Thomas M. Holsen*[2]

1 Institute for a Sustainable Environment, Clarkson University, Potsdam, NY 13676.

2 Department of Civil and Environmental Engineering, Clarkson University, Potsdam, NY 13676.

3 University of Michigan Air Quality Laboratory, Ann Arbor, MI 48109, USA

4 Air Resources Laboratory, U.S. National Oceanic and Atmospheric Administration, College Park, MD 20740

*- holsen@clarkson.edu; 315-268-3851

Site Locations

Figure S1: Map of sampling sites[1]

Data Sources

Underhill, Vermont (VT99) site (44.51N,-72.91W). From Mar. 1992 to July 1999, total gaseous mercury (TGM) and PBM were measured every third day using a Cold Vapor Atomic Fluorescence Spectroscopy (CVAFS) method as previously described by Burke et al.[2] Since only TGM was measured, for trends analysis it was assumed that GEM was equivalent to TGM since the data below support previous findings that the oxidized fraction of the TGM is <2% at remote background monitoring sites.[2, 3] The cut size for PBM is 2.5 µm. From Jun 2004 to Dec. 2008, speciated mercury concentrations were measured using a Tekran model 2537A, 1130, and 1135 and followed early Atmospheric Mercury Network (AMNet) quality assurance protocols.[4, 5] The Jan. 2009 to Dec. 2014 mercury data was collected as part of AMNet and data quality assurance protocol followed the AMNet Data Management Manual.[4]

Huntington Forest, New York (NY20) site (43.97N, -74.22W). Between June 2004 and Dec. 2008 mercury species were measured as documented by Choi, et al.[6] using a Tekran model 2537A, 1130, and 1135 and followed the QA/QC protocols described in that paper. The Jan. 2009 to Dec. 2014 mercury data were produced as part of AMNet and data quality assurance protocols followed the AMNet Data Management Manual.[4, 5]

Potsdam, NY site (44.67N,-74.98W). Daily TGM concentrations were measured from Feb. 2004 to July. 2005 about 0.5 km northwest of a small airport and about 1 km from a main road[7] following the procedures outlined in the US EPA Lake Michigan Mass Balance Methods Compendium.[8] From January Jan. 2013 to Dec. 2014, a Tekran speciation system was operated following the AMNet protocols on the roof of the three story CAMP building at Clarkson University.

Trend analysis method

Kendall's tau test is a nonparametric rank based test [8], which has been widely used in environmental trend analysis.[9, 10] The Kendall's tau test does not assume the data are normally distributed and is less impacted by outliers than most other

methods so it is appropriate for Hg concentration data. Theil-Sen method or Sen's slope was introduced by Thiel[11] and Sen [12] as a non-parametric linear regression model for estimating the slope of the trend in a sample of N pairs of data. It has also been widely used in environmental trend analysis. [13, 14] The Sen's slope is the median of all possible pairwise slopes between points as a trend regression line. The advantage of using the Sen's slope is that it tends to yield accurate confidence intervals even with non-normal data and heteroscedasticity. [15] For each time period and site, the Sen's slope trend yields three slopes: the median, upper 95% confidence interval and lower 95% confidence interval. Kendall's tau test was run using Matlab 2015b (Mathworks) at a 0.05 significance level.

Median values were used in trends analysis to avoid the influence of extreme measurements on the results. Overall trends determined using mean values differed by < 5% of those reported here. Aggregating the data into weekly or monthly medians yielded similar results as using daily medians.

Source Analysis

HYSPLIT modeling was performed with with NOAA EDAS (Eta Data Assimilation System) meteorological data for 2004-2014 and NOAA NARR (North America Regional Reanalysis) meteorological data for 1992 to 1999.[16] The high concentration threshold was set as the upper 10th percentile and a smoothing weight function was applied as described in Han, et al. [17] PSCF calculations were conducted by using new developed Trajectory-based Potential Source Apportionment (TraPSA) Matlab based GUI (http://adweb.clarkson.edu/projects/TraPSA/).

Trends in different seasons
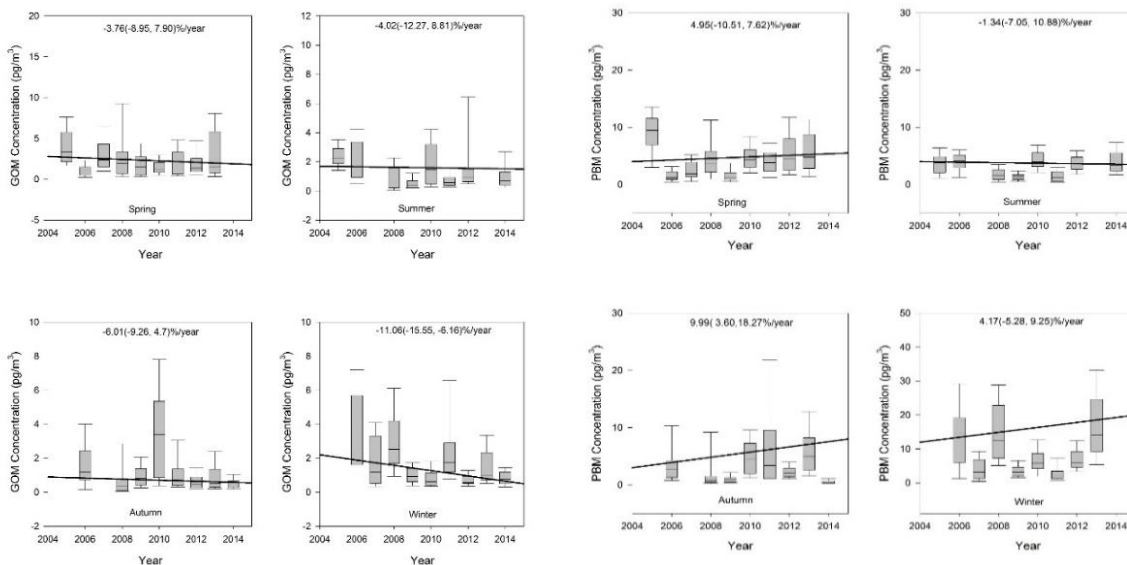

(a)

(b)

(c)

(d)

4
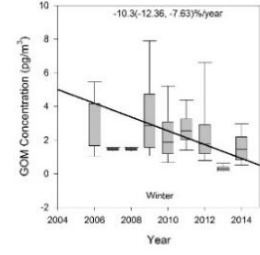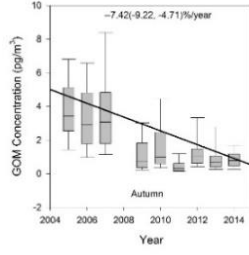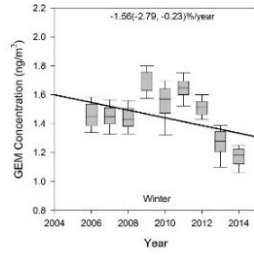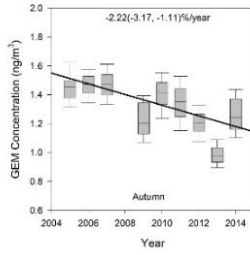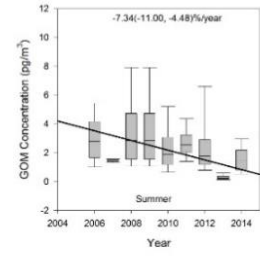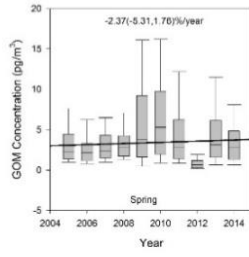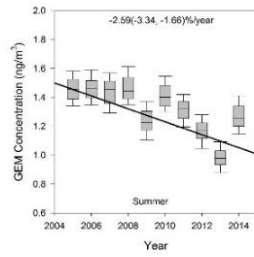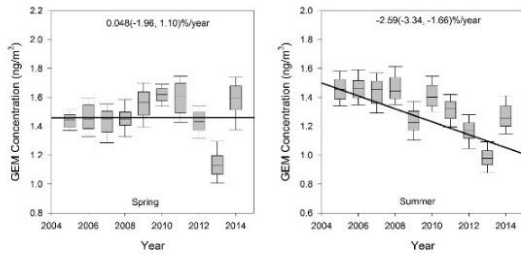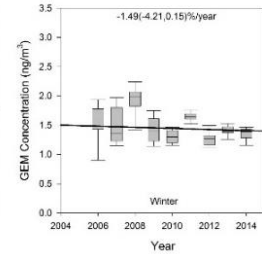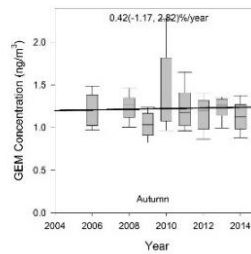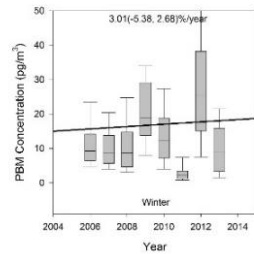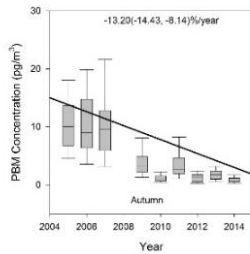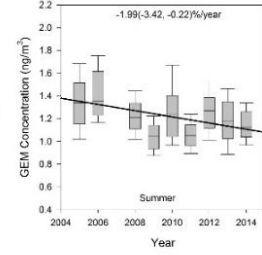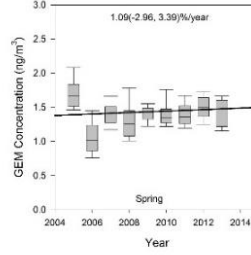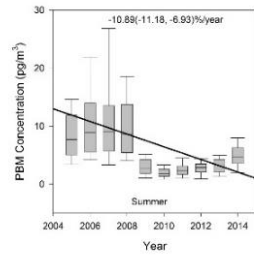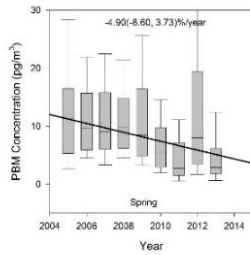
(e)   (f)

Figure S2: Vermont Underhill site (VT99)(a) GEM, (b)GOM, (c) PBM trends and New York Huntington site, (d) GEM, (e) GOM, and (f) PBM from 2004 to 2014 separated by season

Stepwise multiple regression and non-negative least squares regression analysis

Table S1: Stepwise Multiple Regression Results of a) Huntington Forest, NY site and b) Underhill, VT site

	Model	Standardized Coefficients	t	Sig.
1	WV	0.310	6.384	0.000
2	WV	0.228	3.845	0.000
	Year	-0.142	-2.383	0.018
3	WV	0.406	4.172	0.000
	Year	-0.176	-2.888	0.004
	PA	-0.228	-2.296	0.022
4	WV	0.373	3.831	0.000
	Year	-0.117	-1.811	0.071
	PA	-0.360	-3.220	0.001
	OH	0.235	2.501	0.013

(a)

	Model	Standardized Coefficients	T	Sig.
1	Year	-0.425	-10.695	0.000
2	Year	-0.550	-12.330	0.000
	ON	-0.250	-5.606	0.000
3	Year	-0.447	-8.245	0.000
	ON	-0.250	-4.413	0.000
	WV	0.154	3.282	0.001

(b)

[WV]: West Virginia sulfur dioxide emission [Year]: GEM concentration measurement year
[PA]: Pennsylvania sulfur dioxide emission [OH]: Ohio sulfur dioxide emission [ON]: Ontario, Canada sulfur dioxide emission

Non-negative Least Square equation

Year	Huntington Forest, NY	Underhill, VT
2004-2008	[GEM]= 0.00058[Year]+ 0 [CT]+ 0[MD]+ 0 [NY] + 0 [PA]+ 0.0054 [WV]+ 0.0071[OH] + 0 [VA] +0[NJ]	[GEM]= 0.00056 [Year]+ 0 [CT]+ 0[MD]+ 0.0079[NY]+ 0 [PA]+ 0.016[WV]+ 0.0077[OH] + 0.0076 [VA] +0[NJ]
2009-2014	[GEM]= 0.00061 [Year]+ 0.029 [CT]+ 0[MD]+ 0 [NY] + 0[PA]+ 0.0081[WV]+ 0 [OH] + 0 [VA] +0[NJ]	[GEM]= 0.00073[Year] + 0 [CT]+ 0 [MD]+0[NY]+ 0 [PA] + 0 [WV]+ 0 [OH]+ 0 [VA]+0 [NJ]

[GEM]: GEM concentration [Year]: GEM concentration measurement year[CT]: Connecticut sulfur dioxide emission

[MD]: Maryland sulfur dioxide emission[NY]: New York sulfur dioxide emission[PA]: Pennsylvania sulfur dioxide emission

[WV]: West Virginia sulfur dioxide emission [OH]: Ohio sulfur dioxide emission [VA]: Virginia sulfur dioxide emission

[NJ]: New Jersey sulfur dioxide emission

Mercury emissions

Numerous data sets are available to assess spatio-temporal trends in mercury emissions. Each can provide valuable information but each also has limitations. Data sets used in this analysis are summarized in Table S3 and Table S4. Emissions from each of these data sets are shown, for sources within 600 km (Figure S3) and between 600-3000 km (Figure S4) of VT99 (Underhill) and NY20 (Huntington Forest). Because some inventories are not speciated, there are more data shown with *total* Hg emissions (HgT, top-most panels) than for Hg0, Hg2, and HgP emissions in the subsequent panels. Note that even if the inventories were identical in terms of the emissions they represented, some differences would arise due to spatial resolution. For example, depending on the relative positions of grid-square centroids, results for the Zhang et al. inventory (on a 1x1 degree grid) and the AMAP inventory (on a 0.5 x 0.5 degree grid) could seem different, even if the inventories were representing the same underlying data. Likewise, inventories with point sources at explicit latitude and longitudes can show different results from gridded inventories, again, even if the underlying data were identical. Figure S5 shows annual emissions from the USEPA Toxic Release Inventory (TRI) and Environment Canada National Pollutant Release Inventory (NPRI) for the period 2000-2014. Data exist in these inventories for years prior to 2000, but appear to be very incomplete. The data are shown for a variety of distance ranges, i.e., within 200, 300, 600, 1000, 2000, and 3000 km away from the VT99 and NY20 monitoring sites. Note that the "TRI+NPRI" data shown for 0-600 km (panel c) are the same as shown for the "TRI+NPRI" data series in Figures S3 and S4 above.

Table S3: Characteristics of selected emissions inventories to assess spatio-temporal trends in mercury emissions

Emissions Inventory	Coverage	Spatial Resolution	Available years	Speciation	Notes
AMAP/UNEP Global inventory	Global	$0.5° \times 0.5°$	1990; 1995; 2000; 2005; 2010	Yes	• Sector-specific information available • Extensive documentation
Global inventory from Zhang et al. (2016)	Global	$1° \times 1°$	1990; 2000; 2010	Yes	
U.S. EPA National Emissions Inventory (NEI)	U.S.	Point sources with a specific latitude and longitude; area sources specified by U.S. County	1999; 2002; 2005; 2008; 2011	Some point sources speciated <= 2005; 2008 and 2011 inventories are not speciated	• Relatively complete, and subject to some QA/QC procedures • Less frequent updates • Relatively long delay before updated inventories available (e.g., as of Sept 2016, the latest NEI mercury inventory available is for 2011)
U.S. Toxic Release Inventory (TRI)	U.S.	Point sources with a specific latitude and longitude	Annually, from 2000-2014	No	• 1987-1999 data exist but appear to be very incomplete • data since 2000 relatively complete, but not necessarily as comprehensive as NEI; data are generally self-reported by emitters
Canadian National Pollutant Release Inventory (NPRI)	Canada	Point sources with a specific latitude and longitude	Annually, from 2000-2014	No	• 1993-1999 data exist but appear to be relatively incomplete

Table S4: Characteristics of "synthesis" inventories used in HYSPLIT-Hg modeling analyses[9-11]

Project	Coverage	Spatial Resolution	Notes
1990-1996 synthesis, assembled for analysis carried out in Cohen et al. (2004).	U.S. and Canada	• Point sources with a specific latitude and longitude	• U.S. emissions from USEPA data sources represented a range of years from 1990-1996 (and in a few cases, 1999) • Canadian point and area source emissions for 1995
1999-2000 synthesis, assembled for analysis carried out in Cohen et al. (2007).	U.S. and Canada	• Area sources in the U.S. on a county level • Area sources in Canada on a 50km grid in the Great Lakes region, and a 100km grid elsewhere in Canada	• U.S. emissions from USEPA data sources generally representative of 1999, primarily from 1999 NEI • Canadian point source emissions from 2000 NPRI • Canadian area source emissions for 1995, as used in above inventory

2005 synthesis, assembled for analysis carried out in Cohen et al. (2016).	U.S., Canada, global	• Similar to above for U.S. and Canadian point and area sources • Global emissions outside the U.S. and Canada on a 0.5 x 0.5 degree grid	• Point source U.S. emissions from USEPA 2005 NEI • Area source U.S. emissions from USEPA 2002 NEI • Point source Canadian emissions from 2005 NPRI • Area source Canadian emissions for 2000, from 1999-2000 synthesis above • Emissions outside the U.S. and Canada from AMAP 2005 global mercury emissions inventory

Figure S6 shows data for emissions from sources greater than 3000 km away from the sources. In this figure the only data appropriate to show are from the global inventories, as the portions of the US-only (i.e., TRI, NEI) or Canadian-only (i.e., NPRI) inventories further than 3000 km away from the sites are relatively small. Note however that emissions at distances greater than 3000 km within the U.S. and Canada *are* included in the global inventories and are accounted for in this figure.

Figure S7 shows the global, 1º x 1º anthropogenic mercury emissions inventory for 1990, 2000, and 2010 developed and described by Zhang et al. [12] for each year, and for each mercury form (including total Hg), summed over a 3º x 3º grid, for portions of the U.S., Canada, and Mexico. This figure shows this inventory's estimates of the geographical distribution of speciated emissions, and how these change over time. In Figures S8 (for 2005) and S9 (for 2014), emissions from a number of different inventories are summed onto a 1x1 degree grid. In these figures, large point source emissions are shown as scaled circles, as well as being included in the gridded data. Large population centers are also shown in these figures.
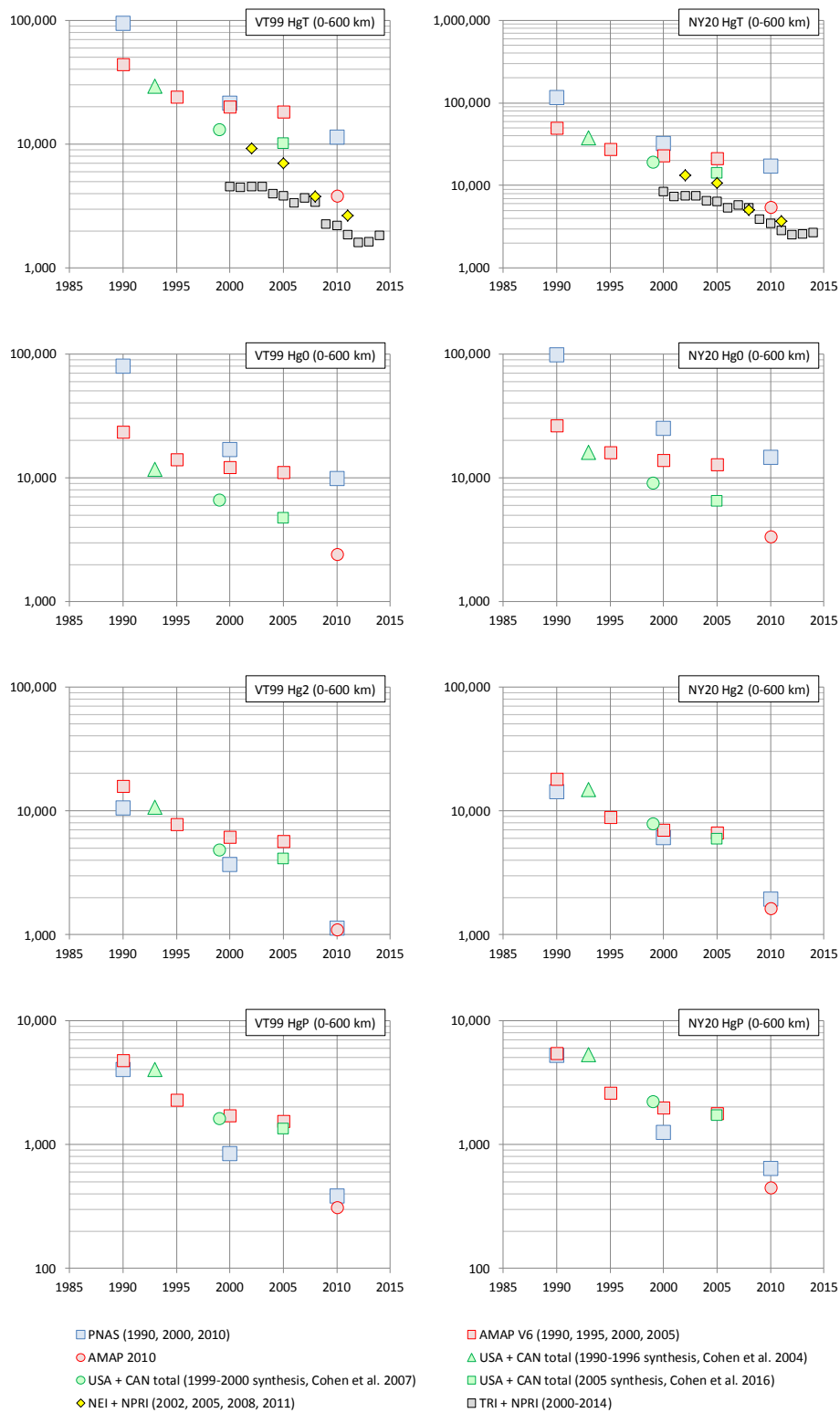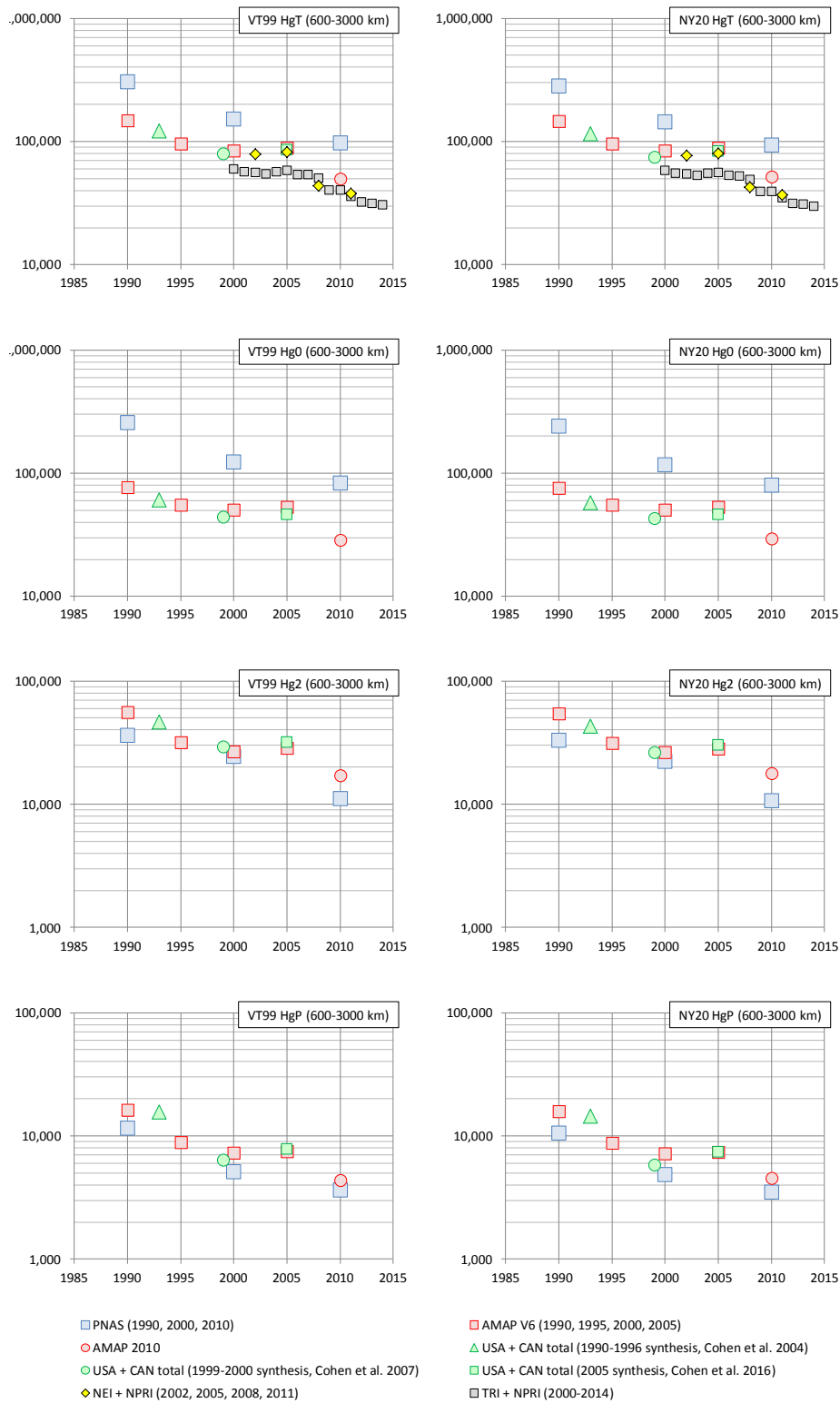
Figure S3: Time trends of direct, anthropogenic mercury emissions (kg/yr) within 600 km of VT99 and NY20. The emissions inventory data sets are described above in Tables S3 and S4. The "PNAS" inventory is from Zhang et al. [12] (published in the *Proceedings of the National Academy of Sciences*).

9

Figure S4: Time trends of direct, anthropogenic mercury emissions (kg/yr) within 600-3000 km of VT99 and NY20. The emissions inventory data sets are described above in Tables S3 and S4. The "PNAS" inventory is from Zhang et al. [12] (published in the *Proceedings of the National Academy of Sciences*).
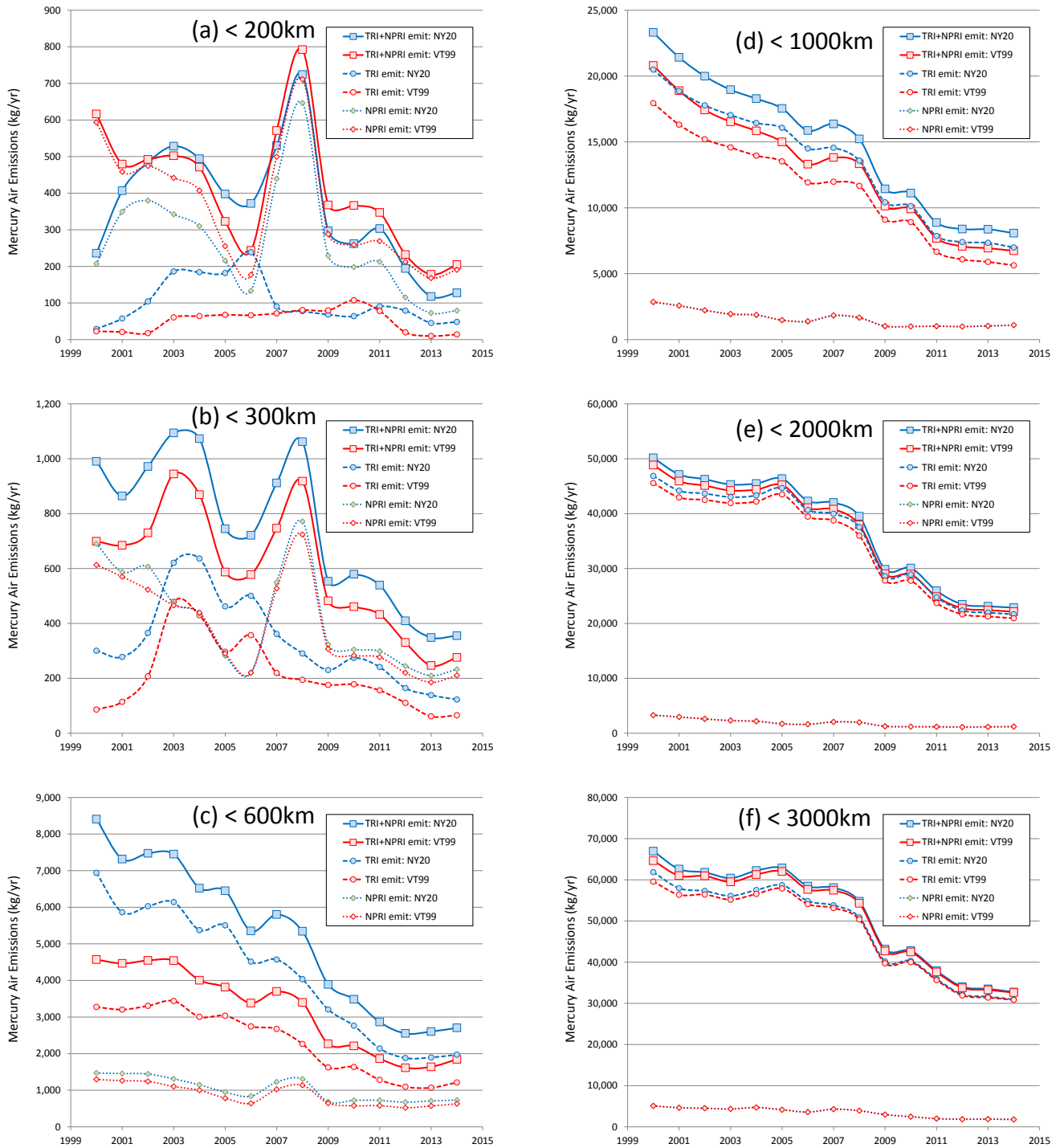
10

Figure S5: Time trends of direct, anthropogenic mercury emissions (kg/yr, linear scale) within different distance ranges of VT99 and NY20: (a) 0-200km, (b) 0-300km, (c) 0-600km, (d) 0-1000km, (e) 0-2000km, and (f) 0-3000km. The emissions inventory data sets are described above in Tables S3 and S4. For the higher distances ranges – (d), (e), (f) – the values for the NPRI emissions (Canadian point sources) are essentially the same for NY20 and VT99. Note that the 2007-2008 peak seen prominently in the 0-200 km (a) and 0-300 km (b) data was primarily because of increased 2008 emissions in Canadian sources within the NPRI. The largest increase that year reported in the NPRI data was for the Clean Harbors waste treatment facility in Mercier Quebec (south of Montreal). Reported Hg emissions from that facility increased from 31 to 527 kg between 2006-2008. Emissions from the facility decreased from 2009-2011, and no Hg emissions have been reported from the facility after 2011.
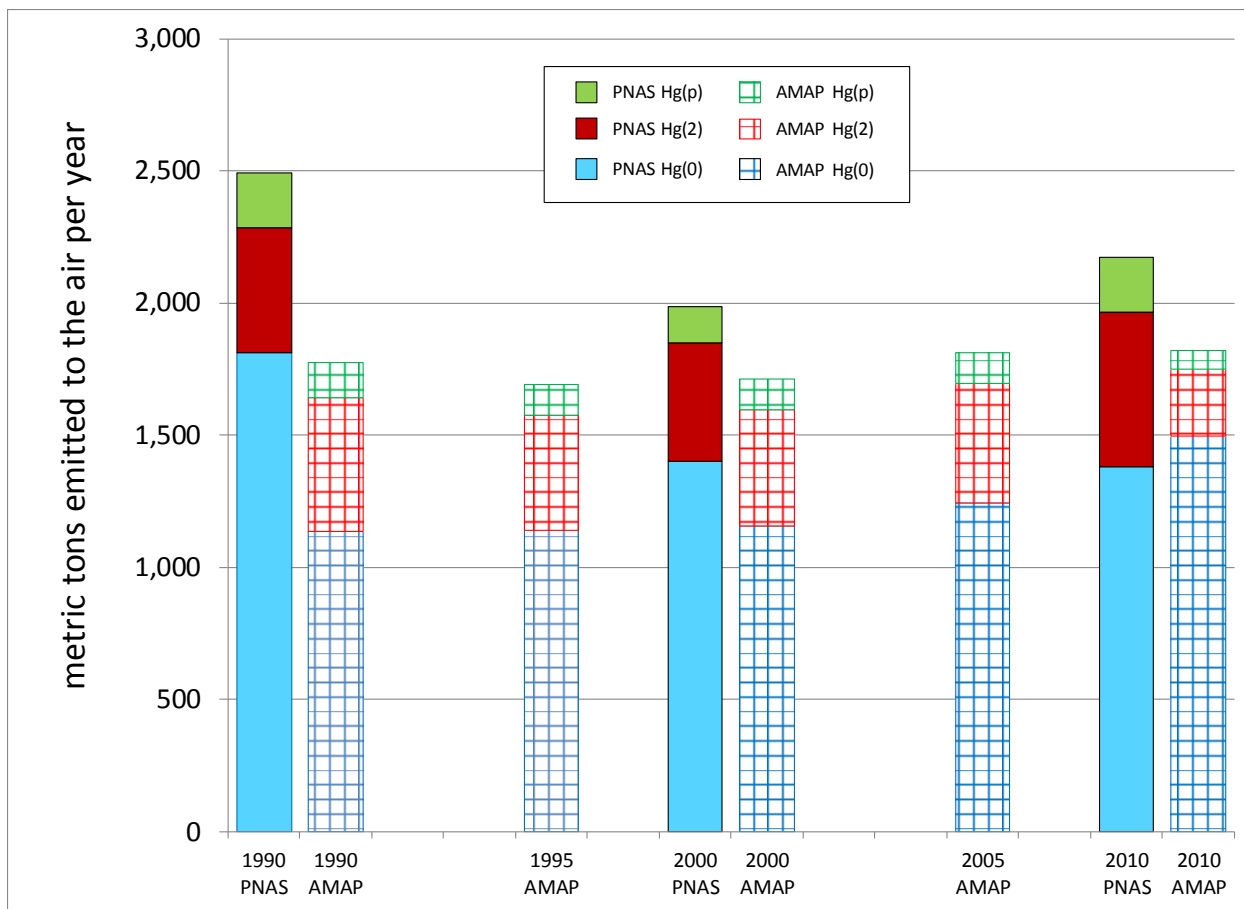
11

Figure S6: Time trends of direct, anthropogenic mercury emissions (metric tons/yr) greater than 3000 km away from VT99 and NY20. The "PNAS" inventory in the above graph refers to the Zhang et al.[12] inventory published in the *Proceedings of the National Academy of Sciences;* the "AMAP" inventory in the above graph refers to the inventory prepared by the Arctic Monitoring and Assessment Programme and UNEP. These emissions inventory data sets are described above in Table S3. Because the sites are relatively close together -- relative to this >3000 km length scale -- the emissions totals for the two sites are essentially identical, and we have shown just one set of time series data. Note that the PNAS inventory only reports emissions for 1990, 2000, and 2010, compared to the 5-year frequency of the AMAP inventory data.
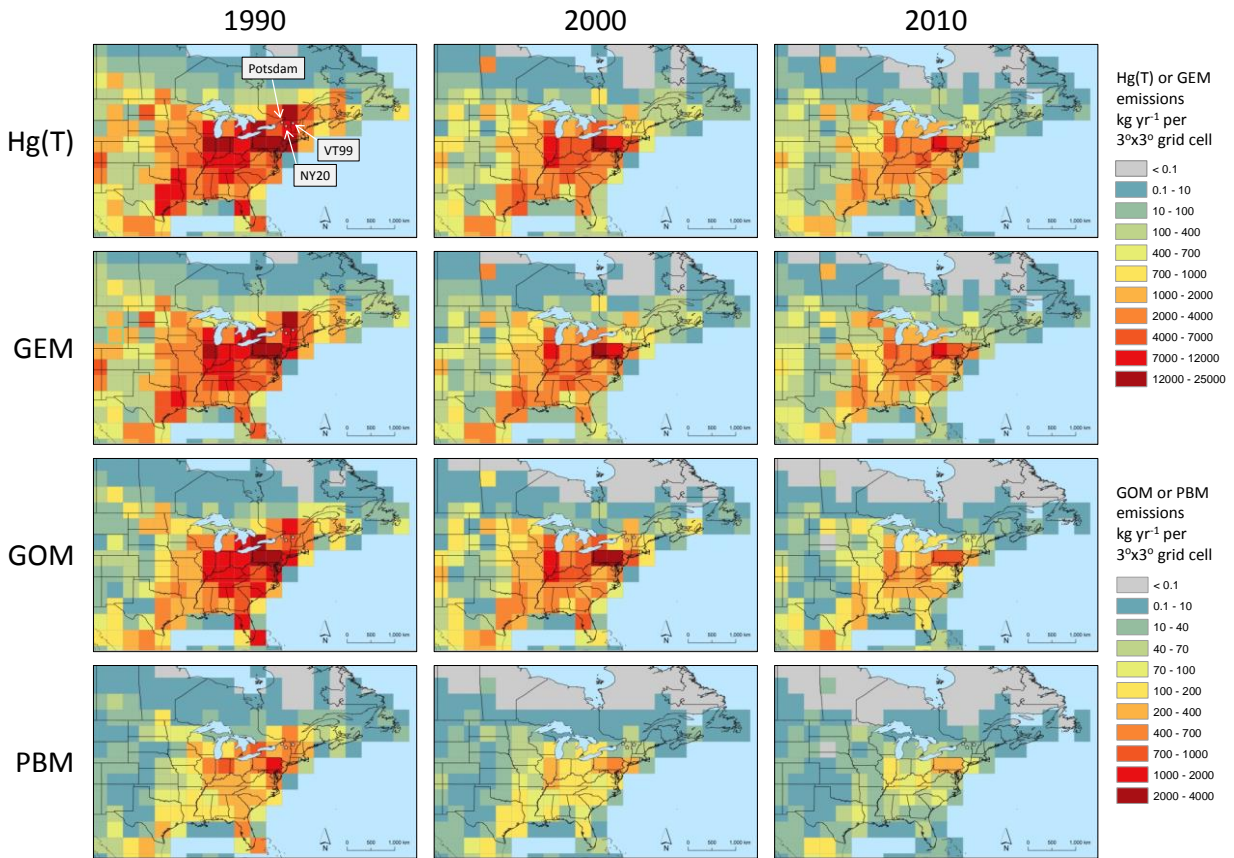
Figure S7: Direct, anthropogenic mercury emissions summed over a 3x3 grid, based on Zhang et al.[12], for total mercury – Hg(T) – and for GEM, GOM, and PBM, for 1990, 2000, and 2010.
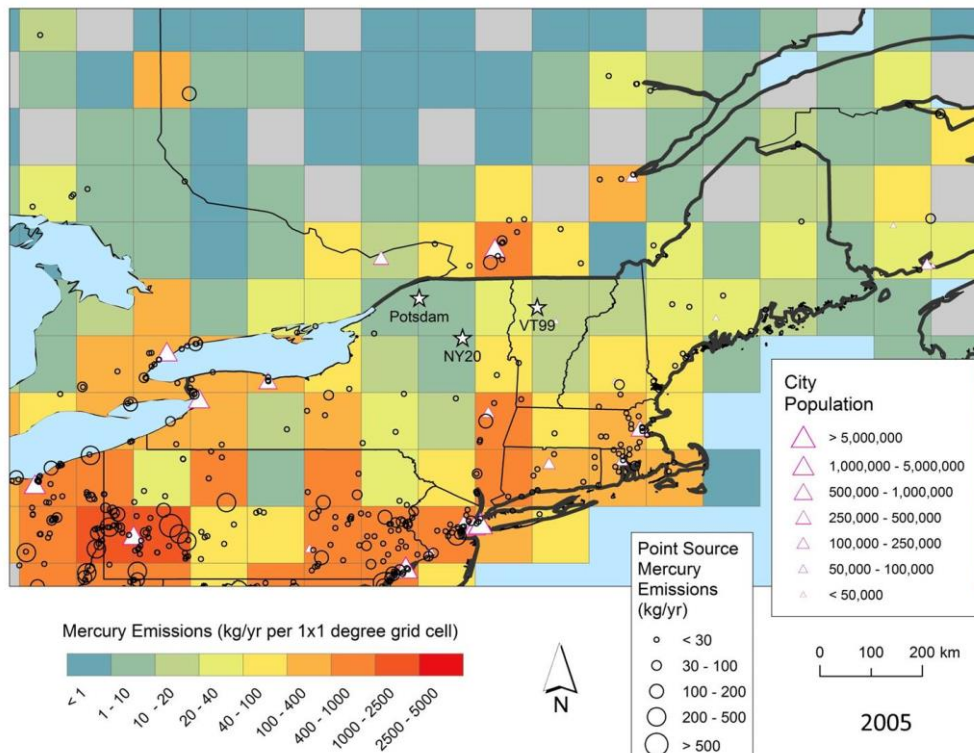
Figure S8: Total, direct anthropogenic mercury emissions, ca. 2005, summed over a 1°x1° grid. Large point source emission sources (included in the grid summation) are shown as scaled circles. Based on inventory described in Cohen et al. (2016).
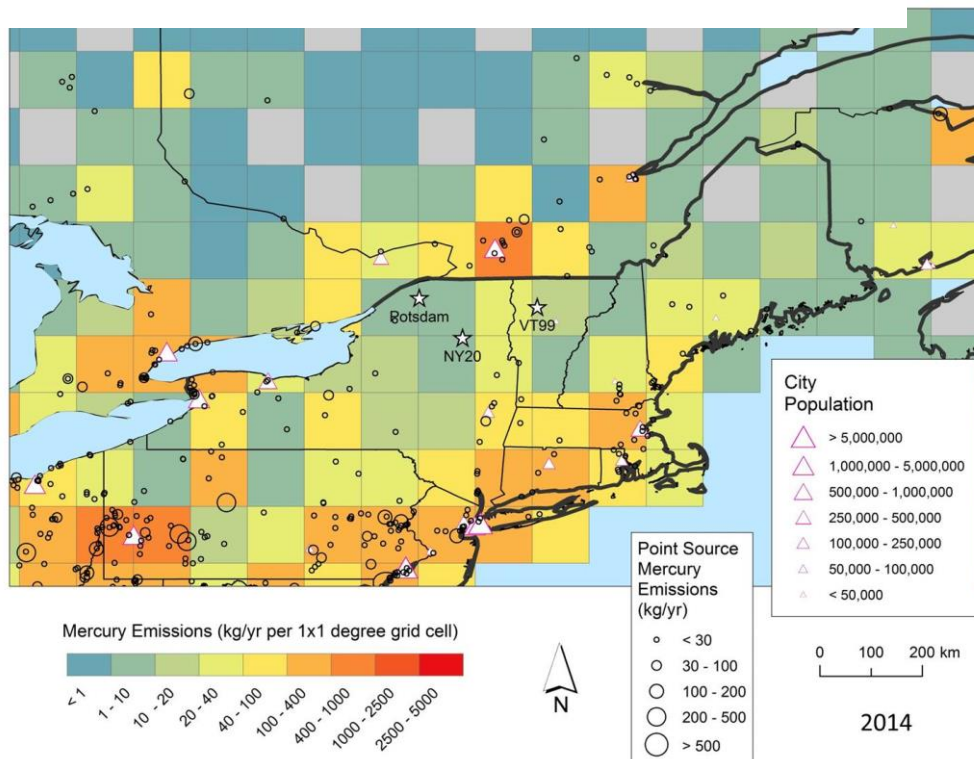

Figure S9: Total, direct anthropogenic mercury emissions, ca. 2014, summed over a 1°x1° grid. Large point source emission sources (included in the grid summation) are shown as scaled circles. Based on USEPA 2014 TRI (U.S. point sources), USEPA 2002 NEI (U.S. area sources), Environment Canada 2014 NPRI (Canadian point sources), and Environment Canada 2000 area sources.
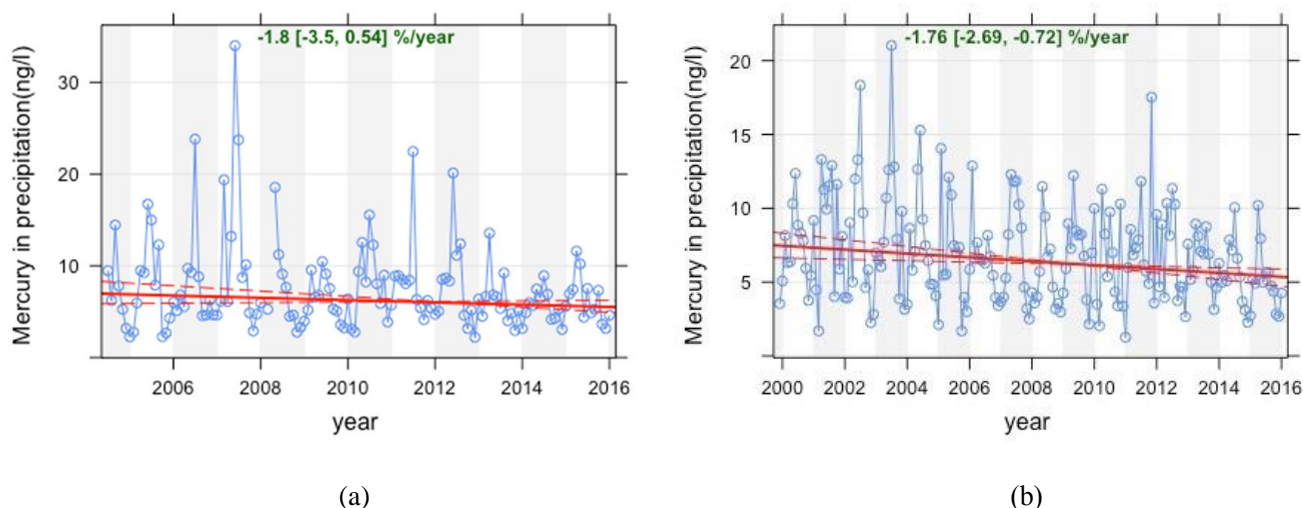
<div align="center">(a)</div>

<div align="center">(b)</div>

Figure S10: Mercury concentration in precipitation trends for the (a) Vermont Underhill site (VT99) and (b) New York Huntington site (NY20). Data from the Mercury Deposition Network (MDN). (p=0.05 and p<0.01 for the VT99 and NY20 sites, respectively)

References:

1.   OnlineAtlas.us, USA State Map. In OnlineAtlas.us: Washinton D.C, 2005.
2.   Burke, J.; Hoyer, M.; Keeler, G.; Scherbatskoy, T., Wet deposition of mercury and ambient mercury concentrations at a site in the Lake Champlain Basin. In *Mercury as a Global Pollutant*, Springer: New York, 1995; pp 353-362.
3.   Gustin, M. S.; Amos, H. M.; Huang, J.; Miller, M. B.; Heidecorn, K., Measuring and modeling mercury in the atmosphere: a critical review. *Atmosphere Chemical Physics* **2015,** *15*, 5697-5713.
4.   Neff, M. R.; Bhavsar, S. P.; Chin, J. X. Y., Spatial and temporal trends of muscle lipid content in Great Lakes fishes: 1970s-2008. *Canadian Journal of Fisheries and Aquatic Sciences* **2012,** *69*, (12), 2007-2017.
5.   NationalAtmosphericDepositionProgram, AtmosphericMercury Network Data Management Manual (2011–12) Version1.9. In 2012.
6.   Choi, H.-D.; Holsen, T. M.; Hopke, P. K., Atmospheric mercury (Hg) in the Adirondacks: Concentrations and sources. *Environmental science & technology* **2008,** *42*, 5644-5653.
7.   Han, Y.-J.; Holsen, T. M.; Lai, S.-O.; Hopke, P. K.; Yi, S.-M.; Liu, W.; Pagano, J.; Falanga, L.; Milligan, M.; Andolina, C., Atmospheric gaseous mercury concentrations in New York State: relationships with meteorological data and other pollutants. *Atmospheric Environment* **2004,** *38*, 6431-6446.
8.   Keeler, G.; Landis, M., Lake Michigan mass balance methods compendium: Standard operating procedure for analysis of vapor phase mercury **1994**.
9.   Cohen, M.; Artz, R.; Draxler, R.; Miller, P.; Poissant, L.; Niemi, D.; Ratte, D.; Deslauriers, M.; Duval, R.; Laurin, R., Modeling the atmospheric transport and deposition of mercury to the Great Lakes. *Environmental Research* **2004,** *95*, 247-265.
10.   Cohen, M.; Artz, R.; Draxler, R. *Report to congress: mercury contamination in the Great Lakes*; EPA-452/R-97-005; 2007.
11.   Cohen, M. D.; Draxler, R. R.; Artz, R. S.; Blanchard, P.; Gustin, M. S.; Han, Y.-J.; Holsen, T. M.; Jaffe, D. A.; Kelley, P.; Lei, H., Modeling the global atmospheric transport and deposition of mercury to the Great Lakes. *Elementa: Science of the Anthropocene* **2016,** *4*, 000118.
12.   Zhang, Y.; Jacob, D. J.; Horowitz, H. M.; Chen, L.; Amos, H. M.; Krabbenhoft, D. P.; Slemr, F.; St Louis, V. L.; Sunderland, E. M., Observed decrease in atmospheric mercury explained by global decline in anthropogenic emissions. *Proceedings of the National Academy of Sciences of the United States of America* **2016,** *113*, 526-31.